

η meson production in NN collisionsK. Nakayama,^{1,2} J. Speth,² and T. -S. H. Lee³¹*Department of Physics and Astronomy, University of Georgia, Athens, Georgia 30602*²*Institut für Kernphysik, Forschungszentrum-Jülich, D-52425 Jülich, Germany*³*Physics Division, Argonne National Laboratory, Argonne, Illinois 60439*

(Received 5 February 2002; published 4 April 2002)

η meson production in both proton-proton and proton-neutron collisions is investigated within a relativistic meson exchange model of hadronic interactions. It is found that the available cross section data can be described equally well by either the vector or pseudoscalar meson exchange mechanism for exciting the $S_{11}(1535)$ resonance. It is shown that the analyzing power data can potentially be very useful in distinguishing these two scenarios for the excitation of the $S_{11}(1535)$ resonance.

DOI: 10.1103/PhysRevC.65.045210

PACS number(s): 25.10.+s, 13.75.-n, 25.40.-h

I. INTRODUCTION

The production of η mesons in nucleon-nucleon (NN) collisions near the threshold energy has been a subject of considerable interest in the past few years, since the existing data are by far the most accurate and complete among those for heavy meson production. Consequently, they provide an opportunity to investigate this reaction in much more detail than any of the other heavy meson production reactions. In addition to the total cross section for the $pp \rightarrow pp\eta$ reaction [1–6], we now have data for $pn \rightarrow pn\eta$ [7] and $pn \rightarrow d\eta$ [5,8] reactions. The differential cross section data for the $pp \rightarrow pp\eta$ reaction [9] are also available. Consequently, there have been a large number of theoretical investigations on these reactions [10–16].

The production of η mesons in NN collisions is thought to occur predominantly through the excitation (and deexcitation) of the $S_{11}(1535)$ resonance, to which the η meson couples strongly. However, the excitation mechanism of this resonance is currently an open issue. For example, Batinić *et al.* [12] have found that both π and η exchanges are the dominant excitation mechanisms. However, they have considered only the $pp \rightarrow pp\eta$ reaction. Fäldt and Wilkin [13] and Gedalin *et al.* [14] have considered both the $pp \rightarrow pp\eta$ and $pn \rightarrow pn\eta$ reactions. In the analysis of Ref. [13] the $pn \rightarrow d\eta$ reaction is also considered. These authors [13,14] find ρ exchange to be the dominant excitation mechanism of the $S_{11}(1535)$ resonance. In particular, it has been claimed [13] that ρ meson exchange is important for explaining the observed shape of the angular distribution of the $pp \rightarrow pp\eta$ reaction. In an analysis of $pp \rightarrow pp\eta$ reaction, Santra and Jain [15] also considered ρ meson exchange as the dominant excitation mechanism of the $S_{11}(1535)$ resonance. In contrast to the findings of Refs. [12–15], Peña *et al.* [16] have found that the dominant contribution arises, not from the $S_{11}(1535)$ resonance current, but from the shorter range part of the nucleonic currents. In this work, we shall report on another possible scenario for exciting the $S_{11}(1535)$ resonance that reproduces both the $pp \rightarrow pp\eta$ and $pn \rightarrow pn\eta$ reactions and discuss the possibility of disentangling these reaction mechanisms.

Although we focus here on the problem just mentioned,

the description of η meson production in NN collisions presents other interesting aspects. For example, the η meson interacts much more strongly with the nucleon than do mesons like the pion so that not only the NN final state interaction (FSI), but also the ηN FSI is likely to play an important role, thereby offering an excellent opportunity to learn about the ηN interaction at low energies. In fact, the near-threshold energy dependence of the observed total cross section for η meson production differs from that of π and η' production, which follow the energy dependence given simply by the available phase space together with the NN FSI. The enhancement of the measured cross section at small excess energies in η production compared to those in π and η' production is generally attributed to the strong attractive ηN FSI. In addition to all of these issues, the theoretical understanding of η meson production in NN collisions near threshold in free space is also required for investigating the dynamics of the $S_{11}(1535)$ resonance in the nuclear medium, the possible existence of ηNN bound states, and the possibility of using η to reveal the properties of high-density nuclear matter created in relativistic heavy-ion collisions.

In Sec. II we introduce our model and define the meson production currents whose details are given in the Appendix. An alternative model, which is similar to previous works based on ρ exchange dominance, is introduced in Sec. III. The results are given in Sec. IV. Section V provides a summary.

II. MESON EXCHANGE MODEL

Our model of the $NN \rightarrow NN\eta$ reaction is based on a relativistic meson exchange model of hadronic interactions. The reaction amplitude is calculated in the distorted wave Born approximation. Here we follow a (nonrigorous but otherwise economic) diagrammatic approach to present our formulation. A more rigorous derivation of the reaction amplitude will be reported elsewhere. We start by considering the meson-nucleon (MN) and NN interactions as the building blocks for constructing the total amplitude describing the $NN \rightarrow NNM$ reaction. We then consider all possible combinations of these building blocks in a topologically distinct way, with two nucleons in the initial state and two nucleons plus a meson in the final state. In this process of constructing

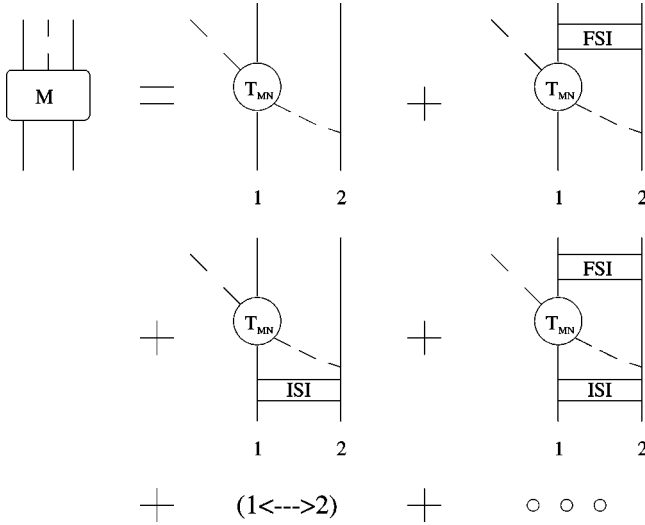


FIG. 1. Amplitude for the $NN \rightarrow NN \eta$ reaction considered in the present work. T_{MN} denotes the MN T matrix. ISI and FSI stand for the initial and final state NN interaction, respectively.

the total amplitude, care must be taken in order to avoid diagrams that lead to double counting. Specifically, the diagrams that lead to mass and vertex renormalizations must be excluded since we choose to use the physical masses and coupling constants. The resulting amplitude constructed in this way is displayed in Fig. 1. The ellipsis indicates those diagrams that are more involved numerically (including, in particular, the MN FSI, which otherwise would be generated by solving the three-body Faddeev equation). So far there are very few attempts to account for them [14,17]. These higher order terms are also not considered in this work.

In order to make use of the available potential models of NN scattering, we will carry out our calculation within a three-dimensional formulation which is deduced from Bethe-Salpeter formulation by restricting the propagating two nucleons to be on their mass shell. We follow the procedure of Blankenbecler and Sugar [18]. The meson production amplitude illustrated in Fig. 1 then takes the following familiar form:

$$M = (1 + T_f^{(-)\dagger} i G_f^{(-)*}) J (1 + i G_i^{(+)} T_i^{(+)}), \quad (1)$$

where $T_{(i,f)}$ denotes the NN T -matrix interaction in the initial (i)/final (f) state, and $G_{(i,f)}$ is the three-dimensional Blankenbecler-Sugar (BBS) propagator. The superscript \pm in $T_{(i,f)}$ as well as in $G_{(i,f)}$ in Eq. (1) indicates the boundary condition, $(-)$ for incoming and $(+)$ for outgoing waves. The production current is denoted by J , which is defined by the MN T matrix with one of the meson legs attached to a nucleon (first diagram on the right-hand side in Fig. 1),

$$J = \sum_{M'} [T_{(MN \leftarrow M'N)}]_1 i P_{M'} [\Gamma_{M'NN}]_2 + (1 \leftrightarrow 2), \quad (2)$$

where $T_{(MN \leftarrow M'N)}$ stands for the MN T matrix describing the transition $M'N \rightarrow MN$, $\Gamma_{M'NN}$ and $P_{M'}$ stand for the $M'NN$ vertex and the corresponding meson propagator, respectively. The subscripts 1 and 2 stand for the two interacting nucleons

1 and 2. The summation runs over the intermediate meson M' . Equation (1) is the basic formula on which the present calculation is based. We note [19] here that care has been taken in the above three-dimensional formulation to avoid double counting problems.

In the near threshold energy region, the two nucleon energy in the final state f is very low and hence the NN FSI amplitude, $T_f^{(-)\dagger}$ in Eq. (1), can be calculated from a number of realistic NN potential models in the literature. In the present work we use the NN model developed by the Bonn group [20] to calculate the FSI. This model is defined by a three dimensionally reduced BBS version of the Bethe-Salpeter equation

$$T = V + ViGT, \quad (3)$$

where G denotes the BBS two-nucleon propagator, consistent with those appearing in Eq. (1) [note that our definition of $V(T)$ differs from that of Ref. [20] by a factor of $-i$].

The NN initial state interaction (ISI) amplitude, $T_i^{(+)}$ in Eq. (1), must be calculated at incident beam energies above 1.25 GeV. There exists no accurate NN model for performing such a calculation. For example, the model developed in Ref. [21] can only give a very qualitative description of the NN scattering phase shifts at energies above 1 GeV. In the present work we therefore follow Ref. [22] and make the on-shell approximation to evaluate the ISI contribution. This amounts to keeping only the δ -function part of the Green function G_i in evaluating the loop integration involving $i G_i^{(+)} T_i^{(+)}$. The required on-shell NN ISI amplitude is obtained from Ref. [23]. As has been discussed in Ref. [22], this is a reasonable approximation to the full NN ISI. In this approximation, the basic effect of the NN ISI is to reduce the magnitude of the meson production cross section. In fact, it is easy to see that the angle-integrated production cross section in each partial wave state i is reduced by a factor of [22]

$$\begin{aligned} \lambda_i &= \left| \frac{1}{2} [\eta_i(p) e^{i2\delta_i(p)} + 1] \right|^2 \\ &= \eta_i(p) \cos^2[\delta_i(p)] + \frac{1}{4} [1 - \eta_i(p)]^2 \\ &\leq \frac{1}{4} [1 + \eta_i(p)]^2. \end{aligned} \quad (4)$$

In the above equation, $\delta_i(p)$ and $\eta_i(p)$ denote the phase shift and corresponding inelasticity, respectively; p stands for the relative momentum of the two nucleons in the initial state.

There are a number of different approaches in the literature which model the production current J defined in Eq. (2) based on meson exchange models. Following Refs. [24,25], we split the MN T matrix of Fig. 1 into the pole (T_{MN}^P) and nonpole (T_{MN}^{NP}) parts and calculate the nonpole part in the Born approximation. Then, the MN T matrix can be written as [26]

$$T_{MN} = T_{MN}^P + T_{MN}^{NP}, \quad (5)$$

where

$$T_{MN}^P = \sum_B f_{MNB}^\dagger g_B f_{MNB}, \quad (6)$$

with f_{MNB} and g_B denoting the dressed meson-nucleon-baryon (MNB) vertex and baryon propagator, respectively. The summation runs over the relevant baryons B . The non-pole part of the T matrix is given by

$$T_{MN}^{NP} = V_{MN}^{NP} + V_{MN}^{NP} i G T_{MN}^{NP}, \quad (7)$$

where $V_{MN}^{NP} \equiv V_{MN} - V_{MN}^P$, with V_{MN}^P denoting the pole part of the full MN potential V_{MN} . V_{MN}^P is given by equation analogous to Eq. (6) with the dressed vertices and propagators replaced by the corresponding bare vertices and propagators. We neglect the second term of Eq. (7) and hence the full MN T matrix in Eq. (2) is approximated as $T_{MN} \approx T_{MN}^P + V_{MN}^{NP}$.

With the approximation described above, the resulting current J consists of baryonic and mesonic currents. The baryonic current is further divided into the nucleonic and nucleon resonance (N^*) currents, so that the total current is written as

$$J = J_{nuc} + J_{res} + J_{mes}. \quad (8)$$

The individual currents are illustrated diagrammatically in Fig. 2. Note that they are all Feynman diagrams and, as such, they include both the positive- and negative-energy propagation of the intermediate particles. The nucleonic current is constructed consistently with the NN potential in the BBS equation (3). The mesonic current consists of the $\eta\rho\rho$, $\eta\omega\omega$, and $\eta a_0\pi$ exchange contributions. The resonance current consists of the $S_{11}(1535)$, $P_{11}(1440)$, and $D_{13}(1520)$ resonances excited via the exchange of π , η , ρ , and ω mesons. Details of our model for the production current are given in the Appendix.

III. VECTOR MESON EXCHANGE DOMINANCE MODEL

In order to allow for a close comparison of the model described in the previous section with the models [13–15] based on ρ meson exchange dominance, we have also constructed a model in which the $S_{11}(1535)$ is excited through the exchange of vector mesons. For this purpose, we follow Refs. [14,15] to define the vector meson couplings with $S_{11}(1535)$ by using the following Lagrangian densities:

$$\mathcal{L}_{\omega NN^*}(x) = -g_{\omega NN^*} \bar{\psi}_{N^*}(x) \gamma_5 \gamma_\mu \omega^\mu(x) \psi_N(x) + \text{H.c.}, \quad (9a)$$

$$\mathcal{L}_{\rho NN^*}(x) = -g_{\rho NN^*} \bar{\psi}_{N^*}(x) \gamma_5 \gamma_\mu \vec{\tau} \cdot [\partial^\nu \vec{\rho}^\mu(x)] \psi_N(x) + \text{H.c.} \quad (9b)$$

Note that the above $\gamma_5 \gamma_\mu$ coupling, which violates gauge invariance, is rather different from the tensor coupling [see

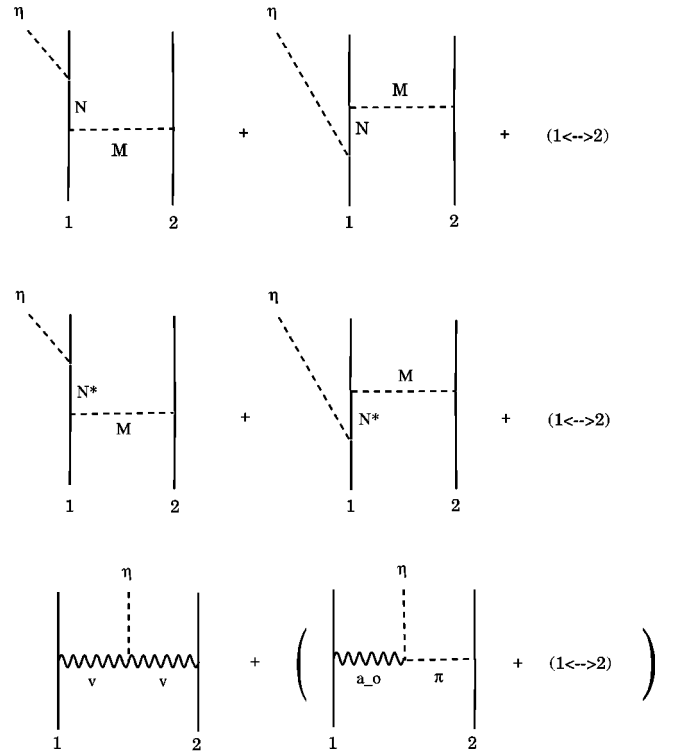


FIG. 2. η meson production currents included in the present study. Upper row: nucleonic current J_{nuc} , $M = \pi, \eta, \rho, \omega, \sigma, a_0$. Middle row: nucleon resonance current J_{res} , $N^* = S_{11}(1535)$, $P_{11}(1440)$, and $D_{13}(1520)$, $M = \pi, \eta, \rho, \omega$. Lower row: mesonic current J_{mes} , $v = \rho, \omega$.

Eqs. (A7c),(A7d)] used in our model described in the previous section and detailed in the Appendix.

In addition to using the $\gamma_5 \gamma_\mu$ coupling in the $vNS_{11}(1535)$ vertex ($v = \rho, \omega$), here we assume the extreme case that $S_{11}(1535)$ is excited exclusively via the exchange of ρ and ω mesons. Furthermore, for simplicity, we neglect all other resonance contributions in the resonance current. This is a reasonable simplification since we find that the resonance current contributions apart from that due to $S_{11}(1535)$ are very small. The nucleonic and mesonic currents are identical to the model described in the previous section. We refer to this model as the vector meson exchange dominance model.

We find that this model can also roughly reproduce the total cross section data by choosing the coupling constants $g_{\rho NN^*} = -0.85$ and $g_{\omega NN^*} = -1.10$ in Eq. (9). Overall, the values of these coupling constants, including the signs, are consistent with those used in Refs. [14,15], in spite of the fact that there the ISI and FSI are treated differently from the present work. We therefore can use this model to investigate the differences between our full model described in Sec. II and the previous works [13–15] based on ρ exchange dominance.

IV. RESULTS

In this section we shall present our results on the η meson production in both the pp and pn collisions based on the

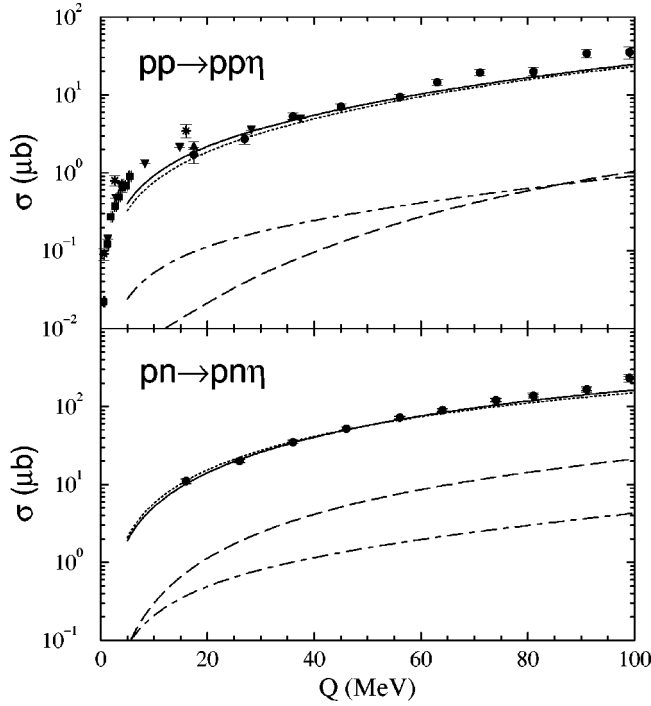


FIG. 3. Total cross sections for the $pp \rightarrow pp\eta$ (upper panel) and $pn \rightarrow pn\eta$ (lower panel) reactions as a function of excess energy within our model described in Sec. II. The dashed curves correspond to the nucleonic current contribution while the dash-dotted curves to the mesonic current contribution; the dotted curves represent the resonance current contribution. The solid curves are the total contribution. The data are from Refs. [1–5,7].

models described in the previous sections. The parameters of the considered models are given explicitly in the Appendix. In short, the coupling constants and range of form factors for meson-baryon-baryon vertices are chosen to be consistent with the Bonn potential in conjunction with the values used in Refs. [24,25] and the values extracted from Particle Data Group [27]. Thus in our calculations there is not much freedom for adjusting parameters.

The total cross sections as a function of excess energy predicted by our model (described in Sec. II) are shown in Fig. 3. The full results are the solid curves which are in general in good agreement with both the data of pp (upper panel) and pn (lower panel) collisions. For small excess energies, our pp results underestimate the data. This is usually attributed to the ηN FSI, which is not accounted for in the present model. Note that the results for $pn \rightarrow pn\eta$ with excess energy $Q > 50$ MeV, corresponding to an incident beam energy larger than 1.3 GeV, should be interpreted with caution, as no reliable NN phase shift analyses for $T=0$ states exist at present for energies above 1.3 GeV [28]. To see the dynamical content of our model, we also show in Fig. 3 the results calculated from keeping only nucleonic current (dashed curves), mesonic current (dash-dotted curves), and resonance current (dotted curves). We see that the total cross sections are obviously dominated by the resonance current, and more specifically by the strong $S_{11}(1535)$ resonance (see Fig. 4). Our nucleonic current contributions (dashed curves) are much smaller than the resonance current contributions.

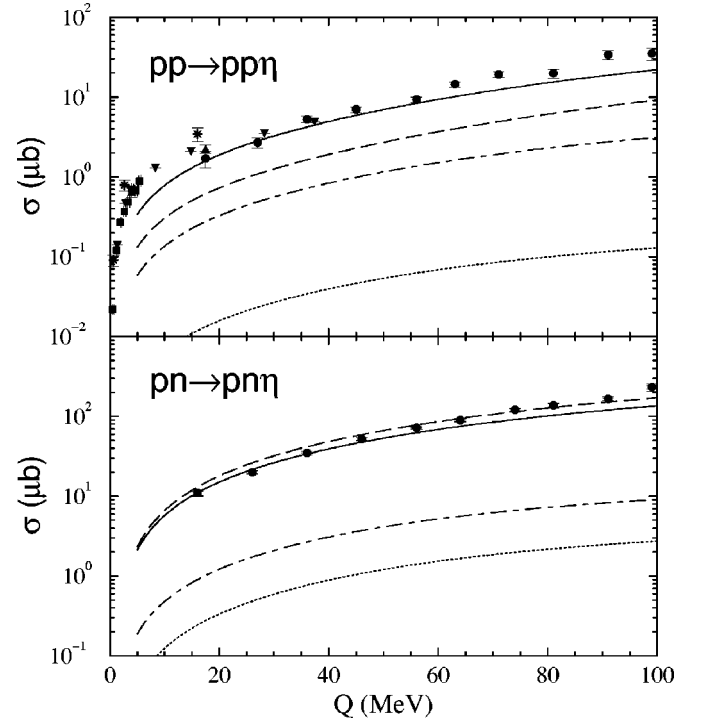


FIG. 4. Same as Fig. 3, except that it shows the $S_{11}(1535)$ resonance contribution only. The dashed curves correspond to the π exchange contribution while the dash-dotted curves to the η exchange contribution; the dotted curves represent the ρ exchange contribution. The solid curves show the total contribution.

This is rather different from the findings of Ref. [16]; there, instead of the resonance current, the shorter range part of the nucleonic current gives a large contribution to the $pp \rightarrow pp\eta$ cross section. It will be interesting to know whether their model can also give a good description of $pn \rightarrow pn\eta$ data, as achieved here (lower panel of Fig. 3).

To examine the differences between our model and previous work, we show in Fig. 4 the results from calculations including only the $S_{11}(1535)$ resonance (solid curves) contribution. Within our model, this resonance excitation is due to the exchange of π , η , ρ , and ω . To see the relative importance between these different meson exchange mechanisms, we also show in Fig. 4 the results from π exchange (dashed curves), η exchange (dash-dotted curves), and ρ exchange (dotted curves). Although the ω exchange is included in the calculation, its contribution is not shown here separately because it is much smaller than the ρ exchange contribution. As can be seen, the dominant contribution is due to π exchange followed by η exchange. The ρ exchange contribution is very small. Several observations are in order here:

(i) In contrast to the result of Refs. [14,15], our model, as given by Eq. (A7d), does not allow the $\gamma^5 \gamma^\mu$ coupling in the ρNN^* vertex for the considered negative parity $S_{11}(1535)$ resonance. Such a coupling would prevent us from determining the ρNN^* coupling from radiative decay $N^* \rightarrow \gamma N$ in the vector meson dominance model (VMD) as explained in the Appendix, since it violates the gauge invariance constraint which is an essential element of VMD. The simplest way of satisfying gauge invariance is to omit the $\gamma^5 \gamma^\mu$ coupling and

TABLE I. Coupling constants g_{MNN^*} used in the resonance current. Those in parentheses for vector mesons refer to $(g_{MNN^*}^{(1)}, g_{MNN^*}^{(2)})$. The ps-pv mixing parameter is fixed to be $\lambda=0$ and the off-shell parameter $z=-1/2$. The masses and widths of the resonances, m_{N^*} and Γ_{N^*} , are in units of MeV.

| N^* (m_{N^*}, Γ_{N^*}) | $S_{11}(1535)$ (1535,150) | $P_{11}(1440)$ (1440,350) | $D_{13}(1520)$ (1520,120) |
|--------------------------------------|------------------------------|------------------------------|------------------------------|
| π | 1.25 | 6.54 | 1.55 |
| η | 2.02 | 0.49 | 6.30 |
| ρ | -0.65 | -0.57 | (6.0, -2.1) |
| ω | -0.72 | -0.37 | (-2.1, 0.7) |

use only the tensor $\gamma^5 \sigma^{\mu\nu}$ coupling, as given in Eq. (A7d). This choice of the ρNN^* coupling, combined with the corresponding coupling constant as given in Table I—which is close to the low limit of the range determined from the measured radiative decay widths—leads to a very small ρ exchange contribution to the cross section as shown in Fig. 4 (dotted curves). This is the main origin of the differences between our results and that of Refs. [14,15] where the ρNN^* vertex for $N^*=S_{11}(1535)$ is specified by the $\gamma^5 \gamma^\mu$ coupling (see also Fig. 6). An alternative to avoid the gauge invariance problem while keeping the $\gamma^5 \gamma^\mu$ term is to use a vertex of the form $\gamma^5 [\gamma^\mu q^2 - (m_{N^*} + m_N) q^\mu]$ [29]. Peña *et al.* [16], on the other hand, have used the vertex $\gamma^5 [\gamma^\mu - (m_{N^*} + m_N) q^\mu / m_\rho^2]$ in conjunction with the coupling constant determined from a quark model [29]. This vertex yields the same meson production amplitude as that of a pure $\gamma^5 \gamma^\mu$ vertex while satisfying the gauge invariance constraint, although only in the on-shell limit ($q^2 = m_\rho^2$). They found a

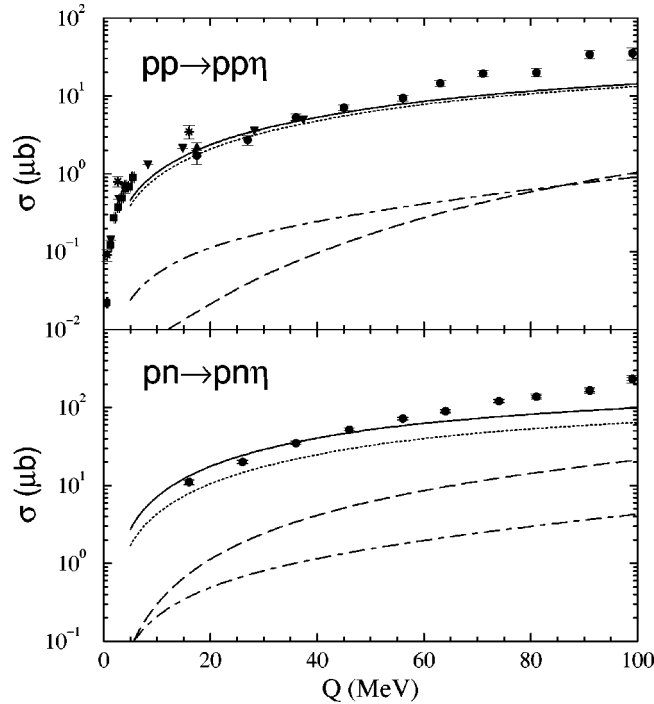


FIG. 5. Same as Fig. 3 but using the vector meson exchange dominance described in Sec. III.

significant contribution of ρ exchange to the excitation of $S_{11}(1535)$ in $pp \rightarrow pp \eta$. Further experimental information is needed to determine whether the $\gamma^5 \gamma^\mu$ coupling is required for vector meson exchange.

(ii) The η exchange contribution is relatively large in the present calculation. In the case of $pp \rightarrow pp \eta$ its contribution to the cross section is about half of that due to the π exchange. The η exchange contribution is subject to a relatively large uncertainty which arises, apart from the introduction of the phenomenological form factors, from the uncertainty in the ηNN coupling strength as discussed in the Appendix. The relatively large contribution of η here results from using the ηNN coupling constant of $g_{\eta NN} = 6.14$, as used in the construction of the Bonn NN interaction [20]. This is close to the upper limit of the range determined empirically as mentioned in the Appendix. However, the η meson exchange in the Bonn potential [20] represents the exchange of a $(J^P, T) = (0^-, 0)$ quantum number and not necessarily of a genuine η meson. On the other hand, the value of $g_{\eta NN} = 6.14$ together with the $\eta - \eta'$ mixing angle of $\theta_P \approx -9.7^\circ$, as suggested by the quadratic mass formula, and the πNN coupling constant of $g_{\pi NN} = 13.45$ leads through SU(3) flavor symmetry to the ratio $D/F \approx 1.43$. This is not too far from the value of $D/F \approx 1.73$ extracted from a systematic analysis of semileptonic hyperon decays [30]. Anyway, in the present calculation for $pp \rightarrow pp \eta$, the η exchange interferes constructively with the dominant π exchange contribution, yielding the total contribution as shown by the solid line in Fig. 4. For $pn \rightarrow pn \eta$, the η exchange interferes constructively with the π exchange in the $T=1$ channel (as in the case of $pp \rightarrow pp \eta$), but destructively in the $T=0$ channel due to the isospin factor -3 in the π exchange amplitude.

(iii) The correct description of both $pp \rightarrow pp \eta$ and $pn \rightarrow pn \eta$ reactions depends not only on the isospin factors associated with the isovector and isoscalar meson exchange but also on a delicate interplay between the NN FSI and ISI in each partial wave. While the NN FSI enhances the total cross section, the NN ISI has an opposite effect (see discussion in Sec. II). In this connection, we mention that in Ref. [13] the reduction factor due to the NN ISI is estimated to be about $\lambda_{(3P_0)} = (0.77)^2 = 0.59$ due to the $3P_0$ state and $\lambda_{(1P_1)} = (0.73)^2 = 0.53$ due to $1P_1$. In our calculation, however, the corresponding reduction factors are about $\lambda_{(3P_0)} = 0.19$ and $\lambda_{(1P_1)} = 0.27$ near the threshold energy. This large discrepancy between the results of Ref. [13] and ours is due to the fact that, whereas our reduction factor is given by Eq. (4), the reduction factor in Ref. [13] is given by $\lambda_i \equiv \eta_i^2 = (e^{-Im(\delta_i)})^2$. We argue that the latter formula is inappropriate for estimating the effect of the NN ISI since it exhibits a pathological feature: namely, when the absorption is maximum ($\eta_i = 0$), this formula yields $\lambda_i = 0$, implying the total absence of the NN elastic channel and thus not allowing the production reaction to occur. However, scattering theory tells us that when the absorption cross section is maximum, the corresponding elastic cross section does not vanish, but is $1/4$ of the absorption cross section. Note that this feature is

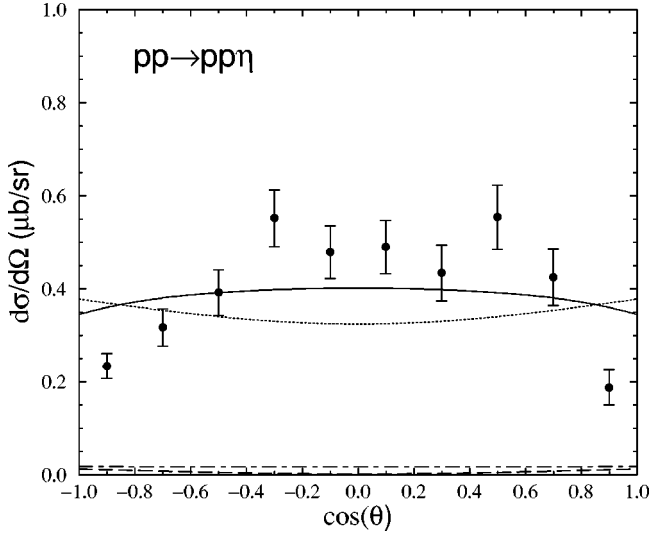


FIG. 6. Angular distribution of the emitted η meson in the c.m. frame of the total system at an excess energy of $Q=37$ MeV. The dashed curve corresponds to the nucleonic current contribution while the dash-dotted curve to the mesonic current contribution; the dotted curves represent the resonance current contribution. The solid curve shows the total contribution. The data are from Ref. [9].

present in Eq. (4). Furthermore, the authors of Ref. [13] apparently have identified incorrectly the inelasticity η_i with $\cos^2(\rho_i)$, where ρ_i is one of the two parameters (the other is the phase shift) given in Ref. [23]. The phase shift parametrization given in Ref. [23] differs from the standard Stapp parametrization. It is obvious that with a more appropriate estimate of the reduction factor λ_i as given by Eq. (4) the result of Ref. [13] would underpredict considerably the cross section data.

We now turn to exploring the vector meson exchange dominance model described in Sec. III. This model does not have the π and η exchange mechanisms for exciting the $S_{11}(1353)$ resonance. The nucleonic and mesonic currents of our full model are kept. With the coupling constants $g_{\rho NN^*} = -0.85$ and $g_{\omega NN^*} = -1.10$ in Eq. (9), we can describe both the $pp \rightarrow pp\eta$ and $pn \rightarrow pn\eta$ data. The results are the solid curves in Fig. 5. In the same figures we also show the contributions from the nucleon resonance (dotted curves) and the nucleonic (dashed curves) and mesonic (dash-dotted curves) currents. Although the total cross section is underpredicted for excess energies $Q > 60$ MeV, it is interesting that these results are in line with the findings of Refs. [13–15].

The results presented above indicate that the total cross section data alone cannot distinguish two different meson exchange mechanisms for the excitation of $S_{11}(1353)$ resonance. It is therefore necessary to consider more exclusive observables. Figure 6 shows the angular distribution (solid curves) of $pp \rightarrow pp\eta$ predicted by our model (described in Sec. II) at an excess energy of $Q=37$ MeV. The data from Ref. [9] are also shown. Again, the resonance contribution (dotted curve) dominates the cross section. As pointed out in Ref. [13], the shape of the angular distribution of the latter contribution bends upwards at the forward and backward angles due to the π exchange dominance in the $S_{11}(1353)$

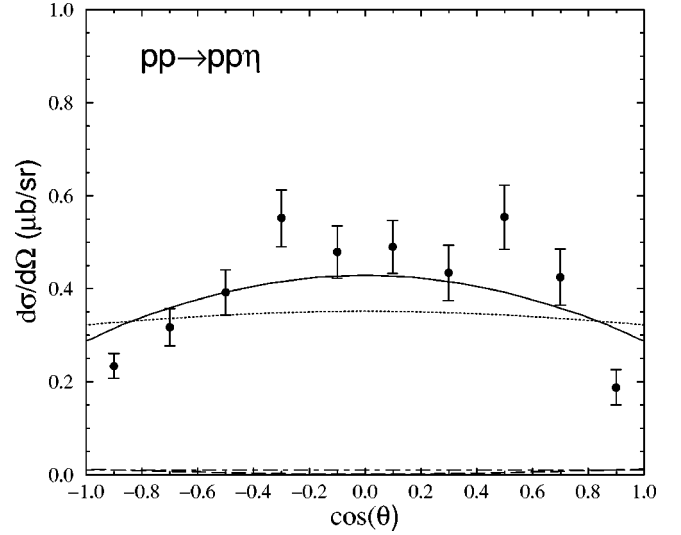


FIG. 7. Same as Fig. 6 but using the vector meson exchange dominance of Sec. III.

resonance contribution. However, due to interference with the nucleonic (dashed) and mesonic (dash-dotted) currents, the shape of the resulting angular distribution (solid curve) is inverted with respect to that of the resonance current contribution alone. As one can see, although the overall magnitude is rather well reproduced, the rather strong angular dependence exhibited by the data is not reproduced by the model described in Sec. II. At this point one might argue that the excitation mechanism of the $S_{11}(1353)$ resonance as given by our model is not correct and that, indeed, the ρ meson exchange is the dominant contribution, as has been claimed in Ref. [13]. This can be studied by considering the predictions of our vector meson exchange dominance model described in Sec. III. The angular distribution predicted by this model is shown in Fig. 7. Here we see that the shape of the calculated angular distribution (solid curve) is in better agreement with the data, although the strong angular dependence exhibited by the data—which shows contributions of higher partial waves than $L=1$ —is not quite reproduced. Judging from the level of agreement between the two predictions and the data, one cannot discard our model in which the $S_{11}(1353)$ is mainly excited by π and η exchange in favor of the ρ exchange dominance model. In this connection, we mention that new data from COSY which will become available soon shows a flat angular distribution [31].

From the above considerations, we conclude that, at present, the excitation mechanism of the $S_{11}(1353)$ resonance in NN collisions is still an open question. Indeed, we have just offered a scenario which is as good as the ρ exchange dominance model in reproducing the available data. It is therefore of special interest to seek a way to disentangle these possible scenarios. In this connection, spin observables may potentially help resolve this issue. As an example, we present in Fig. 8 the analyzing power at $Q=10$ MeV (upper panel) and $Q=37$ MeV (lower panel). The predictions of the present model are shown as the solid curves, whereas the predictions assuming vector meson exchange dominance for exciting the $S_{11}(1353)$ resonance are shown as the dashed

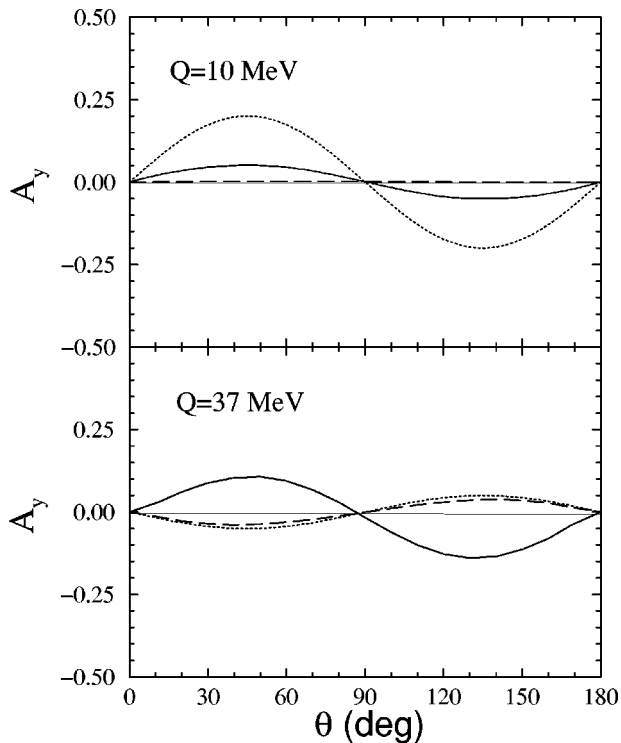


FIG. 8. Analyzing power for the reaction $pp \rightarrow pp \eta$ as a function of emission angle of η in the c.m. frame of the total system at an excess energy of $Q = 10$ MeV (upper panel) and $Q = 37$ MeV (lower panel). The dotted curve corresponds to the case of ρ exchange dominance according to Ref. [13]. The solid curve corresponds to the full model calculation described in Sec. II. The dashed curve is the prediction assuming vector meson exchange dominance as described in Sec. III.

curves. The different features exhibited by the two scenarios for the excitation mechanism of the $S_{11}(1535)$ is evident. According to Ref. [13], the ρ exchange contribution is expected to lead to an analyzing power given by

$$A_y = A_y^{max} \sin(2\theta), \quad (10)$$

where A_y^{max} is positive for low excess energies, peaking at $Q \approx 10$ MeV and becoming negative for excess energies $Q > 35$ MeV. The corresponding results are also shown in Fig. 8 as the dotted curves. Although Eq. (10) gives rise to a larger analyzing power at $Q = 10$ MeV, it is interesting to see that, at $Q = 37$ MeV, it yields a result that nearly coincides with the prediction of the vector meson exchange dominance given in Sec. III.

V. SUMMARY

The production of η mesons in NN collisions has been discussed within a relativistic meson exchange model of hadronic interactions, where the production current has been constructed consistently with the NN FSI used. Special emphasis has been used to investigate the possible excitation mechanisms of the $S_{11}(1535)$ resonance, which is currently a subject of debate. It has been shown that, not only the vector meson dominance for exciting the $S_{11}(1535)$ as advocated by

Wilkin and collaborators [13], but also the excitation mechanism of this resonance mainly via exchange of π and η mesons can describe the existing data in both the pp and pn collisions equally well. We have found that the analyzing power may offer an opportunity to disentangle these reaction mechanisms.

A consistent description of the meson production reaction in pp and pn collisions is not a trivial task. As we have seen, this depends not only on the different isospin factors in the production current which change the relative importance of different reaction mechanisms from pp to pn collisions, but also on a delicate interplay between the NN FSI and ISI. It is clear that the $pp \rightarrow ppM$ and $pn \rightarrow pnM$ as well as the $pn \rightarrow dM$ reaction should be investigated in a consistent way. Also more exclusive observables than the total cross section such as the spin observables should be studied.

Finally, we emphasize that the results presented in this paper should be interpreted with caution. The reason for this is that, as mentioned before, the NN ISI is only accounted for using the on-shell approximation. While this may be a reasonable approximation for calculating cross sections, it may introduce rather large uncertainties in the calculated spin observables. Efforts to improve this will be published elsewhere.

ACKNOWLEDGMENTS

We would like to thank V. Baru, J. Durso, J. Haidenbauer, and C. Hanhart for valuable discussions. We also thank W. G. Love for a careful reading of the manuscript. This work was supported by Forschungszentrum-Jülich, Contract No. 41445282(COSY-58) and by the U.S. Department of Energy, Nuclear Physics Division, Contract No. W-31-109-ENG-38.

APPENDIX: PRODUCTION CURRENTS

The η meson production current consists of nucleonic, mesonic, and resonance currents as shown in Eq. (8) and illustrated diagrammatically in Fig. 2. In the following subsections we construct each of these currents. A general remark to be mentioned here which applies to all of the currents constructed in the following subsections is that, as a consequence of using a three-dimensional reduction of the Bethe-Salpeter equation in evaluating the total amplitude in Eq. (1), the time components of the intermediate particles involved in the production current suffer from an ambiguity in their definitions. In order to be consistent with the NN interaction used in the present work, which has been constructed by using the BBS three-dimensional reduction, the time component of the four-momentum of a virtual meson at the MNN vertex is taken to be $q_o = \varepsilon(l) - \varepsilon(l')$, with $\varepsilon(l)$ and $\varepsilon(l')$ denoting respectively the energies of the nucleon before and after the emission of the virtual meson, $\varepsilon(l) \equiv \sqrt{l^2 + m_N^2}$. The time component of the intermediate baryon in the nucleonic and resonance currents are taken to be $p_o = \omega(k) + \varepsilon(p')$ at the $B \rightarrow M + N$ vertex, while at the $N \rightarrow M + B$ vertex we take $p_o = \varepsilon(p') - \omega(k)$. Here, $\omega(k)$ stands for the energy of the meson produced in the final state.

1. Nucleonic current

The nucleonic current is defined as

$$J_{nuc} = \sum_{j=1,2} (\Gamma_j i S_j U + U i S_j \Gamma_j), \quad (\text{A1})$$

with Γ_j denoting the ηNN vertex and S_j the nucleon (Feynman) propagator for nucleon j . The summation runs over the two interacting nucleons, 1 and 2. U stands for the meson-exchange NN potential. It is, in principle, identical to the potential V appearing in the NN scattering equation, except that here meson retardation effects [which are neglected in the potential entering in Eq. (3)] are kept as given by the Feynman prescription.

The structure of the ηNN vertex Γ_j in Eq. (A1) is derived from the Lagrangian density

$$\mathcal{L}(x) = -g_{\eta NN} \bar{\psi}_N(x) \gamma_5 \left(i\lambda + \frac{1-\lambda}{2m_N} \gamma^\mu \right) \psi_N(x) \partial_\mu \eta(x), \quad (\text{A2})$$

where $g_{\eta NN}$ denotes the ηNN coupling constant and λ is the parameter controlling the pseudoscalar (ps)–pseudovector (pv) admixture. $\eta(x)$ and $\psi_N(x)$ stand for the η and nucleon field, respectively, and m_N denotes the nucleon mass.

The coupling constant $g_{\eta NN}$ is poorly known at present. The empirical values for $g_{\eta NN}$ range anywhere from 1 to 7 [11,20,32,33]. The values extracted from the η photoproduction analysis tend to be in the low side of this range [33], while a value of $g_{\eta NN} = 6.14$ has been used in the NN scattering analysis by the Bonn group [20]. In the present work we use the value of $g_{\eta NN} = 6.14$, consistent with the NN potential V appearing in Eq. (3). Also, we take the pure pseudovector coupling, $\lambda = 0$.

The ηNN vertex derived from Eq. (A2) should be provided with an off-shell form factor. Following Ref. [25], we associate each nucleon leg with a form factor of the following form:

$$F_N(p^2) = \frac{\Lambda_N^4}{\Lambda_N^4 + (p^2 - m_N^2)^2}, \quad (\text{A3})$$

with $\Lambda_N = 1.2$ GeV. p^2 denotes the four-momentum squared of either the incoming or outgoing off-shell nucleon. We also introduce the form factor given by Eq. (A3) at those MNN vertices appearing next to the η -production vertex, where the (intermediate) nucleon and the exchanged mesons are off their mass shell (see Fig. 2). Therefore the corresponding form factors are given by the product $F_N(p^2)F_M(q^2)$, where M stands for each of the exchanged mesons between the two interacting nucleons. The form factor $F_M(q^2)$ accounts for the exchanged meson being off shell and is taken to be consistent with the considered Bonn NN potential used for generating the final NN scattering wave function.

2. Resonance current

The production of η mesons in NN collisions is thought to occur predominantly through the excitation (and de-

excitation) of the $S_{11}(1535)$ resonance, to which the η meson couples strongly. In the present work, we also consider the $P_{11}(1440)$ and $D_{13}(1520)$ resonances.

The resonance current is composed of the spin-1/2 and spin-3/2 resonance contributions

$$J_{res} = J_{res}^{(1/2)} + J_{res}^{(3/2)}. \quad (\text{A4})$$

The spin-1/2 resonance current, in analogy to the nucleonic current, is written as

$$J_{res}^{(1/2)} = \sum_{j=1,2} \sum_{N^*} (\Gamma_{\eta j N^*} i S_{N^*} U_{N^*} + \tilde{U}_{N^*} i S_{N^*} \Gamma_{\eta j N^*}). \quad (\text{A5})$$

Here $\Gamma_{\eta j N^*}$ stands for the ηNN^* vertex function involving the nucleon j . $S_{N^*}(p) = (\not{p} + m_{N^*}) / (p^2 - m_{N^*}^2 + im_{N^*} \Gamma_{N^*})$ is the N^* resonance propagator, with m_{N^*} and Γ_{N^*} denoting the mass and width of the resonance, respectively. The summation runs over the two interacting nucleons, $j=1$ and 2, and also over the spin-1/2 resonances considered, i.e., $N^* = S_{11}(1535)$ and $P_{11}(1440)$. In the above equation U_{N^*} (\tilde{U}_{N^*}) stands for the $NN \rightarrow NN^*$ ($NN^* \rightarrow NN$) meson-exchange transition potential. It is given by

$$U_{N^*} = \sum_{M=\pi,\eta} \Gamma_{MNN^*}(q) i \Delta_M(q^2) \Gamma_{MNN}(q) + \sum_{M=\rho,\omega} \Gamma_{MNN^*}^\mu(q) i D_{\mu\nu(M)}(q) \Gamma_{MNN}^\nu(q), \quad (\text{A6})$$

where $\Delta_M(q^2)$ and $D_{\mu\nu(M)}(q)$ denote the (Feynman) propagator of the exchanged pseudoscalar and vector meson, respectively. $\Gamma_{MNN}(q)$ and $\Gamma_{MNN}^\mu(q)$ denote the pseudoscalar and vector MNN vertex, respectively. These vertices are taken consistently with the NN potential V appearing in Eq. (3) except for the type of coupling at the πNN vertex and the ωNN coupling constant. Following the discussion in Ref. [25], we use the pv coupling ($\lambda = 0$) instead of the ps coupling ($\lambda = 1$) at the πNN vertex. Also, following the discussions in Refs. [24,25,34], the value of the ωNN coupling constant is taken to be $g_{\omega NN} = 11.76$. These exceptions apply to the currents $J_{res}^{(3/2)}$ and J_{mec} as well. An analogous expression to Eq. (A6) holds for \tilde{U}_{N^*} .

Following Ref. [32], the transition vertices Γ_{MNN^*} and $\Gamma_{MNN^*}^\mu$ in Eqs. (A5),(A6) for spin-1/2 resonances are obtained from the interaction Lagrangian densities

$$\mathcal{L}_{\eta NN^*}^{(\pm)}(x) = \mp g_{\eta NN^*} \bar{\psi}_{N^*}(x) \left\{ \left[i\lambda \Gamma^{(\pm)} + \left(\frac{1-\lambda}{m_{N^*} \pm m_N} \right) \Gamma_{\mu}^{(\pm)} \partial^\mu \right] \eta(x) \right\} \psi_N(x) + \text{H.c.}, \quad (\text{A7a})$$

$$\mathcal{L}_{\pi NN^*}^{(\pm)}(x) = \bar{\pi} g_{\pi NN^*} \bar{\psi}_{N^*}(x) \left\{ \left[i\lambda \Gamma^{(\pm)} + \left(\frac{1-\lambda}{m_{N^*} \pm m_N} \right) \Gamma_{\mu}^{(\pm)} \partial^{\mu} \right] \vec{\tau} \cdot \vec{\pi}(x) \right\} \psi_N(x) + \text{H.c.}, \quad (\text{A7b})$$

$$\mathcal{L}_{\omega NN^*}^{(\pm)}(x) = \left(\frac{g_{\omega NN^*}}{m_{N^*} + m_N} \right) \times \bar{\psi}_{N^*}(x) \Gamma^{(\mp)} \sigma_{\mu\nu} [\partial^{\nu} \omega^{\mu}(x)] \psi_N(x) + \text{H.c.}, \quad (\text{A7c})$$

$$\mathcal{L}_{\rho NN^*}^{(\pm)}(x) = \left(\frac{g_{\rho NN^*}}{m_{N^*} + m_N} \right) \times \bar{\psi}_{N^*}(x) \Gamma^{(\mp)} \sigma_{\mu\nu} \vec{\tau} \cdot [\partial^{\nu} \vec{\rho}^{\mu}(x)] \psi_N(x) + \text{H.c.}, \quad (\text{A7d})$$

where $\vec{\pi}(x)$, $\omega^{\mu}(x)$, $\vec{\rho}^{\mu}(x)$, and $\psi_{N^*}(x)$ denote the π , ω , ρ , and spin-1/2 nucleon resonance fields, respectively. The upper and lower signs refer to the even (+) and odd (-) parity resonance, respectively. The operators $\Gamma_{\mu}^{(\pm)}$ and $\Gamma_{\mu}^{(\pm)}$ in the above equations are given by

$$\Gamma^{(+)} = \gamma_5, \quad \Gamma_{\mu}^{(+)} = \gamma_5 \gamma_{\mu},$$

$$\Gamma^{(-)} = 1, \quad \Gamma_{\mu}^{(-)} = \gamma_{\mu}. \quad (\text{A8})$$

The parameter λ in Eqs. (A7a),(A7b) controls the admixture of the two types of couplings: ps ($\lambda=1$) and pv ($\lambda=0$) in the case of an even parity resonance and, scalar ($\lambda=1$) and vector ($\lambda=0$) in the case of an odd parity resonance. On shell, both choices of the parameter λ are equivalent. In this work we take $\lambda=0$. Note that we have not allowed the coupling $\Gamma_{\mu}^{(\mp)}$ in Eqs. (A7c),(A7d) in contrast to Refs. [14,15]. Unlike the νNN vertex ($\nu =$ vector meson), this coupling at the νNN^* vertex prevents us from estimating its strength using the VMD because of the violation of gauge invariance. Although gauge invariant vertices which include the $\Gamma_{\mu}^{(\mp)}$ coupling can be constructed [29], we have omitted this coupling in the present work for simplicity.

Similar to the case of spin-1/2 resonances, the spin-3/2 resonance current is written as

$$J_{res}^{(3/2)} = \sum_{j=1,2} \sum_{N^*} (\Gamma_{\eta j N^*}^{\mu} i S_{\mu\nu(N^*)} U_{N^*}^{\nu} + \tilde{U}_{N^*}^{\mu} i S_{\mu\nu(N^*)} \Gamma_{\eta j N^*}^{\nu}). \quad (\text{A9})$$

Here $\Gamma_{\eta j N^*}^{\nu}$ stands for the ηNN^* vertex function involving the nucleon j .

$$S_{\mu\nu(N^*)}(p) = (\not{p} + m_{N^*}) \{ -g_{\mu\nu} + \gamma_{\mu} \gamma_{\nu} / 3 + (\gamma_{\mu} p_{\nu} - p_{\mu} \gamma_{\nu}) / 3 m_{N^*} + 2 p_{\mu} p_{\nu} / 3 m_{N^*}^2 \} / (p^2 - m_{N^*}^2 + i m_{N^*} \Gamma_{N^*})$$

is the spin-3/2 Rarita-Schwinger propagator. The summation runs over the two interacting nucleons, $j=1$ and 2, and also over the spin-3/2 resonances considered, i.e., $N^* = D_{13}(1520)$ in the present work. In the above equation $U_{N^*}^{\mu}(\tilde{U}_{N^*}^{\mu})$ stands for the $NN \rightarrow NN^*$ ($NN^* \rightarrow NN$) meson-exchange transition potential. It is given by

$$U_{N^*}^{\mu} = \sum_{M=\pi, \eta} \Gamma_{MNN^*}^{\mu}(q) i \Delta_M(q^2) \Gamma_{MNN}(q) + \sum_{M=\rho, \omega} \Gamma_{MNN^*}^{\mu\lambda}(q) i D_{\lambda\nu(M)}(q) \Gamma_{MNN}^{\nu}(q), \quad (\text{A10})$$

where $\Gamma_{MNN^*}^{\mu}(q)$ and $\Gamma_{MNN^*}^{\mu\lambda}(q)$ denote the pseudoscalar and vector MNN^* vertex, respectively. An analogous expression to Eq. (A10) holds for $\tilde{U}_{N^*}^{\mu}$.

The MNN^* vertices involving spin-3/2 nucleon resonances in Eqs. (A9),(A10) are obtained from the Lagrangian densities [32]

$$\mathcal{L}_{\eta NN^*}^{(\pm)}(x) = \left(\frac{g_{\eta NN^*}}{m_{\eta}} \right) \times \bar{\psi}_{N^*}^{\mu}(x) \Theta_{\mu\nu}(z) \Gamma^{(\mp)} \psi_N(x) \partial^{\nu} \eta(x) + \text{H.c.}, \quad (\text{A11a})$$

$$\mathcal{L}_{\pi NN^*}^{(\pm)}(x) = \left(\frac{g_{\pi NN^*}}{m_{\pi}} \right) \times \bar{\psi}_{N^*}^{\mu}(x) \Theta_{\mu\nu}(z) \Gamma^{(\mp)} \vec{\tau} \psi_N(x) \cdot \partial^{\nu} \vec{\pi}(x) + \text{H.c.}, \quad (\text{A11b})$$

$$\mathcal{L}_{\omega NN^*}^{(\pm)}(x) = \bar{\pi} i \left(\frac{g_{\omega NN^*}^{(1)}}{2m_N} \right) \times \bar{\psi}_{N^*}^{\mu}(x) \Theta_{\mu\nu}(z) \Gamma_{\lambda}^{(\pm)} \psi_N(x) \omega^{\lambda\nu}(x) - \left(\frac{g_{\omega NN^*}^{(2)}}{4m_N^2} \right) \times [\partial_{\lambda} \bar{\psi}_{N^*}^{\mu}(x) \Theta_{\mu\nu}(z) \Gamma^{(\pm)} \psi_N(x)] \omega^{\lambda\nu}(x) + \text{H.c.}, \quad (\text{A11c})$$

$$\mathcal{L}_{\rho NN^*}^{(\pm)}(x) = \bar{\pi} i \left(\frac{g_{\rho NN^*}^{(1)}}{2m_N} \right) \times \bar{\psi}_{N^*}^{\mu}(x) \Theta_{\mu\nu}(z) \Gamma_{\lambda}^{(\pm)} \vec{\tau} \psi_N(x) \cdot \vec{\rho}^{\lambda\nu}(x) - \left(\frac{g_{\rho NN^*}^{(2)}}{4m_N^2} \right) [\partial_{\lambda} \bar{\psi}_{N^*}^{\mu}(x) \Theta_{\mu\nu}(z) \times \Gamma^{(\pm)} \vec{\tau} \psi_N(x)] \cdot \vec{\rho}^{\lambda\nu}(x) + \text{H.c.}, \quad (\text{A11d})$$

where $\Theta_{\mu\nu}(z) \equiv g_{\mu\nu} - (z+1/2)\gamma_\mu\gamma_\nu$. In order to reduce the number of parameters, we take $z = -1/2$ in the present work. $\omega^\lambda{}^\nu(x) \equiv \partial^\lambda\omega^\nu(x) - \partial^\nu\omega^\lambda(x)$ and $\vec{\rho}^\lambda{}^\nu(x) \equiv \partial^\lambda\vec{\rho}^\nu(x) - \partial^\nu\vec{\rho}^\lambda(x)$.

The coupling constants g_{MNN^*} used in the present work are displayed in Table. I. They are determined from the centroid values of the extracted decay widths (and masses) of the resonances from Ref. [27] whenever available. Those involving vector mesons, are estimated from the corresponding radiative decay width in conjunction with the VMD. In order to reduce the number of free parameters, the ratio of the $vNN^*(v=\rho,\omega)$ coupling constants for the spin-3/2 $D_{13}(1520)$ resonance has been fixed to be $g_{vNN^*}^{(1)}/g_{vNN^*}^{(2)} = -3$. This is not too far from the ratio of $g_{\gamma NN^*}^{(1)}/g_{\gamma NN^*}^{(2)} = -2.1$ for $N^*=P_{33}(1232)$ extracted from the ratio of $E2/M1 \cong -2.5\%$ as determined from pion photoproduction measurements [35]. As for the coupling constant $g_{vNN^*}(v=\rho,\omega)$ for $N^*=S_{11}(1535)$, we use a value close to the lower limit of the range determined from the radiative decay widths given in Ref. [27] in order to emphasize the pseudoscalar meson exchange dominance in exciting the $S_{11}(1535)$ resonance. Since the $P_{11}(1440)$ resonance is below the ηN threshold, the corresponding coupling constant $g_{\eta NN^*}$ has been determined by folding the results with the mass distribution of the resonance which is assumed to be given by a Breit-Wigner form. The signs of the coupling constants are chosen consistently with those used in the π and η photoproduction analysis [32,36].

Following Ref. [25] and, in complete analogy to the nucleonic current, we introduce the off-shell form factors at each vertex involved in the resonance current. We adopt the same form factor given by Eq. (A3), with m_N replaced by m_{N^*} at the MNN^* vertex, in order to account for the N^* resonance being off-shell. The MNN^* vertex, where the exchanged meson is also off-shell, is multiplied by an extra form factor $F_M(q^2)$ in order to account for the off shellness of this meson [see Eqs. (A6),(A10)]. The corresponding full form factor is therefore given by the product $F_N(p^2)F_M(q^2)$, where M stands for the exchanged meson between the two interacting nucleons. The form factor $F_M(q^2)$ is taken consistently with the NN potential V in Eq. (3); the only two differences are the normalization point of $F_v(q^2)(v=\rho,\omega)$ and the cutoff parameter value of $F_\pi(q^2)$. Here, the form factor for vector mesons $F_v(q^2)$ is normalized to unity at $q^2=0$ in accordance with the kinematics at which the coupling constant g_{vNN^*} was extracted, i.e., $F_v(q^2) = [\Lambda_v^2/(\Lambda_v^2 - q^2)]^2$. For the pion form factor $F_\pi(q^2)$, following the discussion in Refs. [24,25,34], we use the cutoff value of $\Lambda_\pi = 0.9$ GeV. We also use this value of the cutoff in the form factor at the πNN vertex in Eqs. (A6),(A10) as well as in the πNN vertex appearing in the mesonic current constructed in the next subsection.

3. Mesonic current

For the meson-exchange current we consider the contribution from the $\eta\nu\nu$ vertex with ν denoting either a ρ or ω meson. This gives rise to the dominant meson-exchange cur-

rent. The $\eta\nu\nu$ vertex required for constructing the meson-exchange current is derived from the Lagrangian densities

$$\begin{aligned}\mathcal{L}_{\eta\rho\rho}(x) &= -\frac{g_{\eta\rho\rho}}{2m_\rho}\varepsilon_{\alpha\beta\nu\mu}[\partial^\alpha\vec{\rho}^\beta(x)]\cdot[\partial^\nu\vec{\rho}^\mu(x)]\eta(x), \\ \mathcal{L}_{\eta\omega\omega}(x) &= -\frac{g_{\eta\omega\omega}}{2m_\omega}\varepsilon_{\alpha\beta\nu\mu}[\partial^\alpha\omega^\beta(x)][\partial^\nu\omega^\mu(x)]\eta(x),\end{aligned}\tag{A12}$$

where $\varepsilon_{\alpha\beta\nu\mu}$ is the Levi-Civita antisymmetric tensor with $\varepsilon_{0123} = -1$. The vector meson-exchange current is then given by

$$\begin{aligned}J_{\eta\nu\nu} &= \sum_{v=\rho,\omega} \{[\Gamma_{vNN}^\alpha(k_v)]_1 iD_{\alpha\beta}(k_v)\Gamma_{\eta\nu\nu}^{\beta\mu} \\ &\quad \times (k_v, k'_v) iD_{\mu\nu}(k'_v)[\Gamma_{vNN}^\nu(k'_v)]_2\},\end{aligned}\tag{A13}$$

where $D_{\alpha\beta}(k_v)$ and $D_{\mu\nu}(k'_v)$ stand for the (Feynman) propagators of the two exchanged vector mesons (either the ρ or ω mesons as $v=\rho$ or ω) with four-momentum k_v and k'_v , respectively. The vertices involved in the above equation are self-explanatory. The vNN vertex $\Gamma_{vNN}^\mu(v=\rho,\omega)$ is taken consistently with those in the potential used for constructing the NN T matrix in Eq. (3). The ωNN coupling constant is, however, taken to have the same value mentioned in the previous subsection.

The coupling constant $g_{\eta\nu\nu}$ is determined from a systematic analysis of the radiative decay of pseudoscalar and vector mesons in conjunction with VMD. This is done following Refs. [24,25,37], with the aid of an effective Lagrangian with SU(3) flavor symmetry and imposition of the Okuba-Zweig-Iizuka rule [38]. The parameters of this model are the angle $\alpha_\nu(\alpha_\rho)$, which measures the deviation from the vector (pseudoscalar) ideal mixing angle, and the coupling constant of the effective SU(3) Lagrangian. They are determined from a fit to radiative decay of pseudoscalar and vector mesons. The parameter values determined in this way in Ref. [37] (model B), however, overpredict the measured radiative decay width of the η' meson [27]. Therefore we have readjusted slightly the value of the coupling constant of the SU(3) Lagrangian in order to reproduce better the measured widths. We have $\alpha_\nu \cong 3.8^\circ$ and $\alpha_\rho \cong -45^\circ$, as given by the quadratic mass formula, and the coupling constant of the effective SU(3) Lagrangian of $G=7$ in units of $1/\sqrt{m_\nu m'_\nu}$, where m_ν and m'_ν stand for the mass of the two vector mesons involved. The sign of the coupling constant G is consistent with the sign of the $\rho\pi\gamma$ and $\omega\pi\gamma$ coupling constants taken from an analysis of the pion photoproduction data in the ~ 1 -GeV energy region [39]. With these parameter values we obtain

$$\begin{aligned}g_{\eta\rho\rho} &= G \cos(\alpha_\rho) = 4.94, \\ g_{\eta\omega\omega} &= -G[\sqrt{2}\sin^2(\alpha_\nu)\sin(\alpha_\rho) + \cos^2(\alpha_\nu)\cos(\alpha_\rho)] \\ &= 4.84.\end{aligned}\tag{A14}$$

The $\eta v v$ vertex ($v = \rho, \omega$) in Eq. (A13), where the exchanged vector mesons are both off their mass shells, is accompanied by a form factor. Following Refs. [24,25], we assume the form

$$F_{\eta v v}(k_v^2, k_v'^2) = \left(\frac{\Lambda_v^2 - m_v^2}{\Lambda_v^2 - k_v^2} \right) \left(\frac{\Lambda_v^2}{\Lambda_v^2 - k_v'^2} \right). \quad (\text{A15})$$

It is normalized to unity at $k_v^2 = m_v^2$ and $k_v'^2 = 0$, consistent with the kinematics at which the value of the coupling constant $g_{\eta v v}$ was determined. We adopt the cutoff parameter value of $\Lambda_v = 1.45$ GeV as determined in Ref. [24] from the study of the ω and ϕ meson production in pp collisions. This form factor has been also used in the study of the η' meson production in Ref. [25].

Another potential candidate for mesonic current is the $\eta a_o \pi$ -exchange current, whose coupling constant may be estimated from the decay width of a_o into an η and π . We take the Lagrangian density

$$\mathcal{L}_{\eta a_o \pi}(x) = \frac{g_{\eta a_o \pi}}{\sqrt{m_{a_o} m_\pi}} \vec{a}_o(x) \cdot [\partial_\mu \vec{\pi}(x)] [\partial^\mu \eta(x)], \quad (\text{A16})$$

where $\vec{a}_o(x)$ stand for the a_o meson field. m_π and m_{a_o} stand for the masses of the π and a_o meson, respectively. Using the measured decay width from Ref. [27] we obtain a value of $|g_{\eta a_o \pi}| \approx 1.81$. The sign of this coupling constant is not fixed. We assume it to be positive in the present work. Since the contribution of the $\eta a_o \pi$ current is small, the sign of its

coupling constant will not affect the major conclusion of the present work.

The $\eta a_o \pi$ current reads

$$J_{\eta a_o \pi} = \{ [\Gamma_{a_o NN}]_1 i \Delta_{a_o}(k_{a_o}^2) \Gamma_{\eta a_o \pi} \times (k_{a_o}, k_\pi) i \Delta_\pi(k_\pi^2) [\Gamma_{\pi NN}(k_\pi)]_2 \} + (1 \leftrightarrow 2) \quad (\text{A17})$$

in our previously defined notation. The vertex $\Gamma_{a_o NN}$ is taken consistently with that in the NN potential V in Eq. (3), while for the πNN vertex we use the same one (including the cutoff parameter value) mentioned in the previous subsection. The $\eta a_o \pi$ vertex, $\Gamma_{\eta a_o \pi}(k_{a_o}, k_\pi)$, is assumed to have a form factor given by

$$F_{\eta a_o \pi}(k_{a_o}^2, k_\pi^2) = \left(\frac{\Lambda_{a_o}^2 - m_{a_o}^2}{\Lambda_{a_o}^2 - k_{a_o}^2} \right) \left(\frac{\Lambda_\pi^2 - m_\pi^2}{\Lambda_\pi^2 - k_\pi^2} \right) \quad (\text{A18})$$

with $\Lambda_{a_o} = \Lambda_\pi = 1.45$ GeV.

The total mesonic current is then given by

$$J_{mec} = \sum_{v=\rho, \omega} J_{\eta v v} + J_{\eta a_o \pi}. \quad (\text{A19})$$

There are, of course, other possible mesonic currents, such as the $\eta \omega \phi$ - and $\eta \phi \phi$ -exchange currents, that contribute to η meson production in NN collisions. Their contributions have been estimated in a systematic way following Ref. [24] and were found to be negligible.

-
- [1] E. Chiavassa *et al.*, Phys. Lett. B **322**, 270 (1994).
 [2] F. Hibou *et al.*, Phys. Lett. B **438**, 41 (1998).
 [3] H. Calén *et al.*, Phys. Lett. B **366**, 39 (1996).
 [4] J. Smyrski *et al.*, Phys. Lett. B **474**, 182 (2000).
 [5] H. Calén *et al.*, Phys. Rev. Lett. **79**, 2642 (1997).
 [6] B. Tatischeff *et al.*, Phys. Rev. C **62**, 054001 (2000).
 [7] H. Calén *et al.*, Phys. Rev. C **58**, 2667 (1998).
 [8] H. Calén *et al.*, Phys. Rev. Lett. **80**, 2069 (1998).
 [9] H. Calén *et al.*, Phys. Lett. B **458**, 190 (1999).
 [10] J.M. Laget, F. Wellers, and J.F. Lecomte, Phys. Lett. B **257**, 254 (1991); T. Vetter, A. Engel, T. Biró, and U. Mosel, *ibid.* **263**, 153 (1991); M.P. Rekaló, J. Arvieux, and E. Tomasi-Gustafsson, Phys. Rev. C **55**, 2630 (1997); A. Sibirtsev and W. Cassing, Eur. Phys. J. A **2**, 333 (1998); E. Gedalin, A. Moalem, and L. Rzdolskaja, Nucl. Phys. **A650**, 471 (1999); V.Yu. Grishina *et al.*, Phys. Lett. B **475**, 9 (2000).
 [11] V. Bernard, N. Kaiser, and U. Meißner, Eur. Phys. J. A **4**, 259 (1999).
 [12] M. Batinić, A. Svarc, and T.-S.H. Lee, Phys. Scr. **56**, 321 (1997).
 [13] G. Fäldt and C. Wilkin, Phys. Scr. **64**, 427 (2001), and references therein.
 [14] E. Gedalin, A. Moalem, and L. Rzdolskaja, Nucl. Phys. **A634**, 368 (1998).
 [15] A.B. Santra and B.K. Jain, Nucl. Phys. **A634**, 309 (1998).
 [16] M.T. Peña, H. Garcilazo, and D.O. Riska, Nucl. Phys. **A683**, 322 (2001).
 [17] A. Moalem, L. Rzdolskaja, and E. Gedalin, hep-ph/9505264.
 [18] R. Blankenbeckler and R. Sugar, Phys. Rev. **142**, 1051 (1966).
 [19] We note that if the full two-nucleon propagator is used, the amplitude in Eq. (1) would have an additional term to avoid the double counting which otherwise would arise from the terms involving $iG_i^{(+)}T_i^{(+)}$ and/or $T_f^{(-)\dagger}iG_f^{(-)*}$ and the nucleonic current J_{nuc} as given in Eq. (8) and constructed explicitly in the Appendix (see also Fig. 2). This additional term vanishes if the full two-nucleon propagator is approximated by a three dimensionally reduced propagator $G_{(if)}$ which restricts the energies of the propagating two nucleons onto their respective mass-shell energies.
 [20] R. Machleidt, Adv. Nucl. Phys. **19**, 189 (1989).
 [21] A. Matsuyama and T.-S.H. Lee, Phys. Rev. C **34**, 1900 (1986).
 [22] C. Hanhart and K. Nakayama, Phys. Lett. B **454**, 176 (1999).
 [23] Extracted from the Data Analysis Center, Center for Nuclear Studies (http://gwdac.phys.gwu.edu/analysis/nn_analysis.html).
 [24] K. Nakayama *et al.*, Phys. Rev. C **60**, 055209 (1999).
 [25] K. Nakayama *et al.*, Phys. Rev. C **61**, 024001 (1999).
 [26] B.C. Pearce and I.R. Afnan, Phys. Rev. C **34**, 991 (1986).

- [27] Particle Data Group, C. Caso *et al.*, Eur. Phys. J. C **3**, 1 (1998).
[28] I. Strakovsky (private communication).
[29] D.O. Riska and G.E. Brown, Nucl. Phys. **A679**, 577 (2001).
[30] F.E. Close and R.G. Roberts, Phys. Lett. B **316**, 165 (1993); P.G. Ratcliffe, *ibid.* **365**, 383 (1996); X. Song, P.K. Kabir, and J.S. McCarthy, Phys. Rev. D **54**, 2108 (1996).
[31] K. Kilian (private communication).
[32] M. Benmerrouche, N.C. Mukhopadhyay, and J.F. Zhang, Phys. Rev. D **51**, 3237 (1995); J.F. Zhang, N.C. Mukhopadhyay, and M. Benmerrouche, Phys. Rev. C **52**, 1134 (1995).
[33] L. Tiator, C. Bennhold, and S.S. Kamalov, Nucl. Phys. **A580**, 455 (1994); M. Kirchbach and L. Tiator, *ibid.* **A604**, 385 (1996); S. Neumeier and M. Kirchbach, Int. J. Mod. Phys. A **15**, 4325 (2000); W.-T. Chiang, S.N. Yang, L. Tiator, and D. Drechsel, Nucl. Phys. **A700**, 429 (2002).
[34] K. Nakayama *et al.*, Phys. Rev. C **57**, 1580 (1998).
[35] G. Blanpied *et al.*, Phys. Rev. Lett. **79**, 4337 (1997); R. Beck *et al.*, Phys. Rev. C **61**, 035204 (2000).
[36] T. Feuster and U. Mosel, Nucl. Phys. **A612**, 375 (1997); A. Yu. Korchin, O. Scholten, and R.G.E. Timmermans, Phys. Lett. B **438**, 1 (1998).
[37] J.W. Durso, Phys. Lett. B **184**, 348 (1987).
[38] S. Okubo, Phys. Lett. **5**, 165 (1963); G. Zweig, CERN Report No. TH412 1964; J. Iizuka, Suppl. Prog. Theor. Phys. **37&38**, 21 (1966).
[39] H. Garcilazo and E. Moya de Guerra, Nucl. Phys. **A562**, 521 (1993).